# Shrinkage Analysis Considering Expansion and Contraction Behavior in Heavy Section Spheroidal Graphite Iron Castings

Yutaka Miyamoto
Ube Steel Co., Ltd., Ube, Japan

Haruki Itofuji
Adstefan Casting Solution Center, Tohoku University, Sendai, Japan



## ABSTRACT

The volumetric expansion/contraction behavior of heavy section spheroidal graphite iron castings during solidification was examined via computer simulation to predict the existence of shrinkage cavities. To accurately grasp and quantify the expansion/contraction behavior, actual solidification curve was divided into regions at the inflection points. And then, each region was given the theoretical amount of volumetric expansion and contraction according to Fe-C system equilibrium diagram. The qualified values were adopted as the analytical factor for simulation software. The calculation results showed good matching to the actual shrinkage behavior such as the position and quantity.

**Keywords:** spheroidal graphite iron, heavy section, CAE, simulation, shrinkage

## INTRODUCTION

Shrinkage cavities formed in spheroidal graphite iron casting had been dependent on the shape and dimension in practice[1-3]. These cavities have been generally simulated by hand calculation using formulas[4,5] described below;

Casting modulus Mc (cm) = Volume/surface of area
Shape factor, F = (width + Length)/Thickness
Riserless index I (cm) = Mc / F

Recently, computer simulation has been introduced in practice[6-13]. Niyama criterion[6] has been the most popular for shrinkage analysis in current indices. However, it's not enough for applying to spheroidal graphite iron castings yet because the simulation results are not accurate enough. The reason is that they are using soft wares for steel, aluminum, magnesium, etc. like taking only shrink type solidification. There had been almost no software which was considered the volumetric expansion and contraction behavior. Even if software was considered the behavior, it was insufficient. Therefore, analytical results had not been in matching to the actual shrinkage phenomena in practice.

In this study, an innovative simulation method, which was considered the theoretical amount of volumetric expansion and contraction on solidification curve, was attempted.

## DESIGN OF EXPERIMENTS

### PREPARATION OF TEST BLOCKS

At first, sample castings were poured into furan sand mold and the solidification curves were measured.  After shaking out from mold, samples were cut at their center and their section quality were surveyed. Fig. 1 shows the casting design for cubic and plate blocks. The size of the cubic blocks was determined such that the casting modulus (Mc = volume / surface area) value ranges from 1 to 5 and 10cm (0.4 to 1.97 and 3.9in.). The length of one side was Mc × 60 mm (2.36 in.). The size of the plate blocks was 220 mm (8.66 in.) × 300 mm (11.81 in.) × 70 mm (2.76 in.), (Width × Length × Thickness). It was produced based on the riserless design. In a chiller design, two chill blocks of 50 mm (1.97 in.) × 100 mm (3.94 in.) × 50 mm (1.97 in.) (Width × Length × Thickness) were placed in the upper and lower molds, respectively. A neck-down riser of 240 mm (9.45 in.) × 240 mm (9.45 in.) was placed in the riser design. The mold was made by mixing recycled silica sand with 0.8 wt % furan resin (relative to the sand) and 40 wt % catalyst (relative to the resin).

10ton low-frequency induction furnace was used for melting. Product return materials were employed as the melting material. After melting down, the chemical composition was adjusted at 1450C (2642F), and the base molten iron was super-heated at over 1500C (2732F) for 5 min.  Subsequently, it was naturally cooled and tapped. The spherization and inoculation processes were performed using a sandwich method wherein 1.2 wt % Fe-45mass%Si-5.5mass%Mg alloy, 0.3 wt % Fe-75mass%Si alloy, and 2.0 wt % cover materials (Steel scrap chips) were placed in order in the casting ladle. The solidification curve was measured using a Ø0.3mm (0.01in.) K type thermocouple sheathed with Ø1.6mm (0.06in.) Inconel was inserted into a Ø5.0mm (0.19in.) O. D× Ø3.0mm (0.11in.) I. D silica tube. Thereafter, the thermocouples were placed at the center of thickness and the center of the side face of cubic block. Meanwhile, the plate block was placed at the center of thickness.

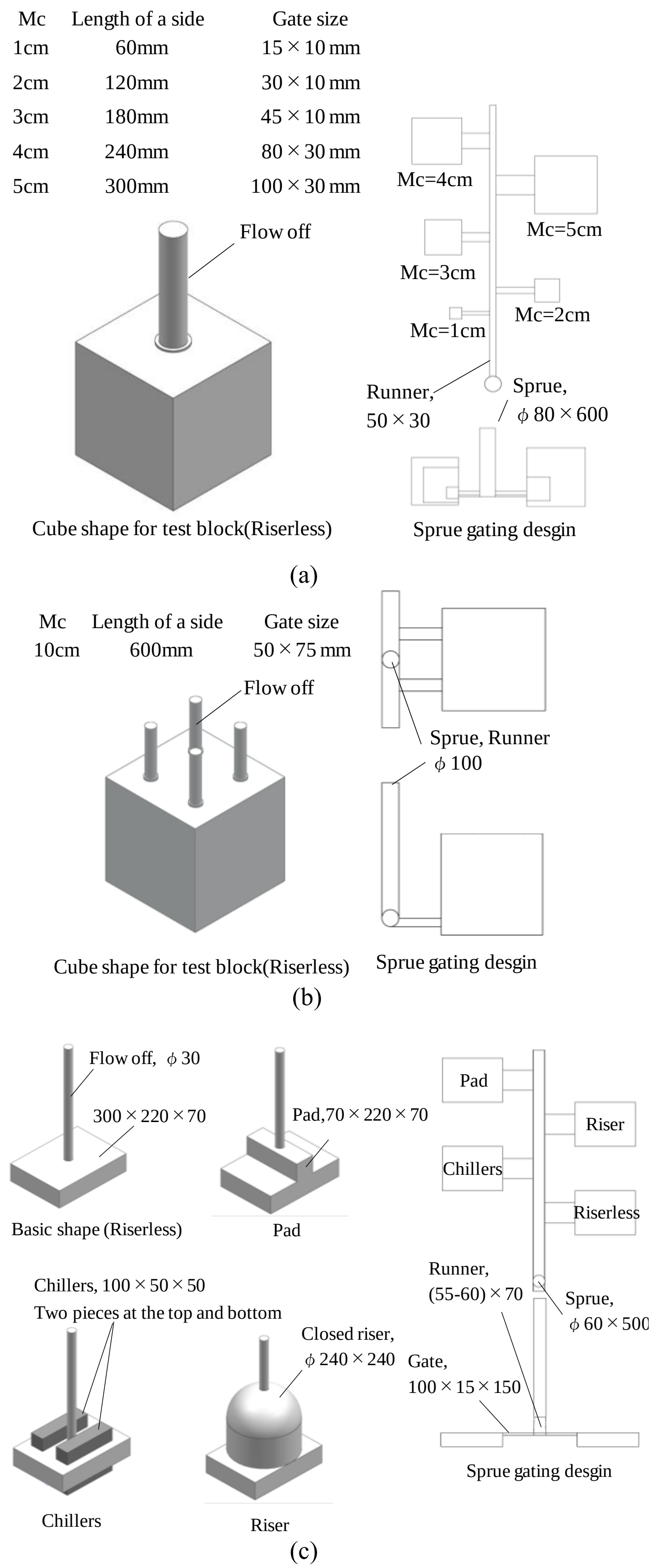


***Fig. 1 These casting designs were used in preparation of test blocks; View(a) cubic blocks, Mc=1-5cm; (b) cubic block, Mc=10cm; (c) plate blocks.***

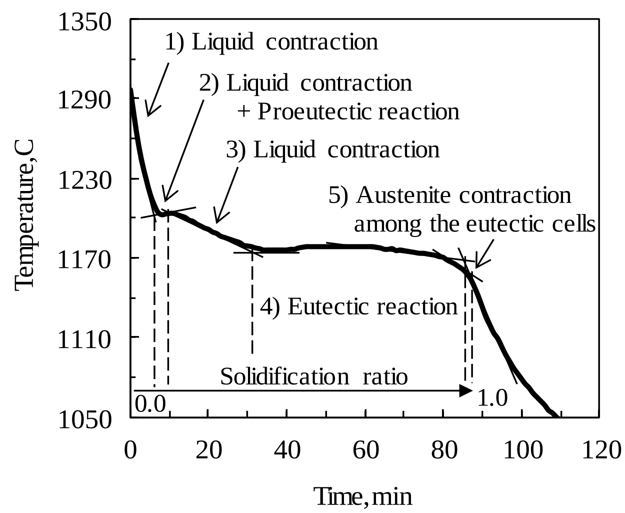


***Fig. 2 shows the inflection points were determined by a tangent-line method and solidification ratio were determined for each point, for example.***

In confirming the shrinkage cavities existence, another identical mold was prepared without K type thermocouple of cubic blocks. And the casting was successively performed.

## SHRINKAGE CAVITY ANALYSIS

The prediction of the existence of the shrinkage cavities in this study was performed by quantitatively determining the expansion/contraction behavior during the solidification and applying the results to the casting simulation. First, the proportion of the reaction time in the total solidification time were obtained. The reactions occurring from the beginning of the casting to the end of the solidification were in the following order: 1) liquid contraction, 2) proeutectic reaction and liquid contraction, 3) liquid contraction 4) eutectic reaction, and 5) austenite contraction among the eutectic crystal cells. The start and end points of each reaction were determined by reading the inflection points in the measured solidification curve. The tangent method was adopted to determine the inflection point, and the percentage of the reaction was calculated assuming that the solidification ratio of 0.0% is at the finish point of pouring and at the starting point of solidification also, as shown in Fig.2. Measurement for inflection point can also use the first derivative curve.

Subsequently, the theoretical volume change was calculated by substituting the amount of carbon/silicon and the initial temperature of the cast at the end of the casting into Eqn.1.[4]

$$TV = Sl + Epg(or\ Sp\gamma) + Eeg + Se\gamma \qquad \text{Eqn.1}$$

Where: TV = volumetric change, Sl = liquid shrinkage (vol %), Epg = expansion of proeutectic graphite (vol %), Spγ = contraction of proeutectic austenite (vol %), Eeg = expansion of eutectic graphite (vol %), contraction of eutectic austenite (vol %)

In the above equations, Epg was used when the chemical composition was hypereutectic and Sp$\gamma$ was used when the composition was hypoeutectic. These values may be determined by the following equations:

$$Sl = \left[\frac{(Ti-1423)}{100}\right] \times 1.5 \qquad \text{Eqn.2}$$

$$Epg = \left[\frac{(Cx-Ce)}{(100-Ce)}\right] \times 3.4 \times 100 \qquad \text{Eqn.3}$$

$$Sp\gamma = -3.5 \times \left[\frac{(Ce-Cx)}{(Ce-C\gamma)}\right] \qquad \text{Eqn.4}$$

$$Eeg = \left[\frac{(1-Sl)}{100}\right] \times \left[\frac{(100-Cx)}{(100-Ce)}\right] \times \left[\frac{(Ce-C\gamma)}{(100-C\gamma)}\right] \times 3.4 \times 100 \qquad \text{Eqn.5}$$

$$Se\gamma = -3.5 \times 100 \times \left[\frac{(1-Sl)}{100}\right] \times \left[\frac{(100-Cx)}{(100-Ce)}\right] \times \left[\frac{(100-Ce)}{(100-C\gamma)}\right] \qquad \text{Eqn.6}$$

Where: Ti = Initial temperature of the molten metal in the mold (C), Ce = Carbon content at the eutectic point (mass%), Cx = Carbon content of the molten metal (mass%), C$\gamma$ = Carbon solid solution content in austenite (mass%), 3.5 = Shrinkage ratio of austenite, 3.4[1] = Density ratio of austenite / graphite

Here, the liquid contraction was assumed to be 1.5 vol% per 100 C[1, 2, 13, 14]. Other equations were used the lever rules in the equilibrium state diagram. Furthermore, Ce and C$\gamma$ were determined by the following equations:

$$Ce = 4.27 + \frac{Si}{3} \qquad \text{Eqn.7}$$

$$C\gamma = 2.045 - 0.178 \times Si \qquad \text{Eqn.8}^{15}$$

Where: Si = Silicon content in the molten metal (mass%)

Finally, the amount of expansion/contraction in each reaction was divided by the ratio of the corresponding reaction to calculate the degree of expansion/contraction. Hence, the expansion/contraction behavior was quantified. The actual calculation results will be reported later.

The software used for the casting simulation is the ADSTEFAN Ver. 2016 made by the Hitachi Industry & Control Solutions, Ltd. The calculated values of the expansion/contraction behavior were inputted into the software to obtain the filled ratio of the materials in which only the contraction occurs, such as a cast steel[16]. In this function, the amount of shrinkage cavity is calculated by multiplying the solid phase rate and shrinkage factor together considering the molten metal flow. This analytical predictions regarding the solidification shrinkage were expressed as indices, which are named I&M's Criterion in this study. The physical properties and boundary conditions used in the solidification analysis are shown in Table 1. In this table, the initial values in the analysis software and the general values. The element division of the three-dimensional model was uniformly set to 5 mm (0.19 in.).

***Table 1. Physical properties and heat transfer parameters.***

| | Casting | Mold | Chill | Sleeve |
|---|---|---|---|---|
| Density (kg/m$^3$) | 7000 | 1550 | 7850 | 650 |
| Specific heat (kJ/(kg·K)) | 1.047 | 1.047 | 0.670 | 0.921 |
| Thermal conductivity（W/(m·K)) | 20.93 | 1.05 | 33.49 | 0.46 |
| Latent heat (kJ/kg) | 209 | - | - | - |
| Heat transfer coefficient (W/(m$^2$·K)) | Casting/Mold : 4186.2<br>Casting/Chiller : 1395.4<br>Casting/Sleeve : 837.2<br>Mold/Chiller : 8372.4<br>Mold/Sleeve : 837.2 | | | |

## EXPERIMENTAL RESULTS AND DISCUSSION

### CASTING OF TEST BLOCKS

#### Pouring results

Table 2 shows the obtained chemical compositions of the test blocks upon completion of the pouring. Yield of Mg was satisfactory.

***Table 2. Chemical composition of test blocks (mass%)***

| Block Shape | C | Si | Mn | P | S | Mg | CE |
|---|---|---|---|---|---|---|---|
| Cube (Mc=1-5) | 3.39 | 2.26 | 0.31 | 0.051 | 0.010 | 0.049 | 4.14 |
| Cube (Mc=10) | 3.25 | 2.31 | 0.26 | 0.052 | 0.01 | 0.048 | 4.02 |
| Plate | 3.31 | 2.38 | 0.30 | 0.057 | 0.011 | 0.059 | 4.10 |

#### Solidification curve

Fig. 3 and 4 show the solidification cooling curves for the cubic and plate blocks, respectively. In these blocks, the total solidification time increased with the increase in the block volume. The results showed that the temperature was accurately measured.

Fig. 5 shows the solidification rate of the cubic test block. The solidification rate was calculated dividing the distance between the surface and the center by the start and end time of the eutectic reaction at the surface and center of the blocks. The start and end times of this solidification was obtained from the solidification curves. The solidification rate decreased with increasing Mc value for both the start and end of eutectic solidification. It is assumed that due to mushy solidification, as the solidification rate increases, the difference becomes smaller in the solidification time between surface and center; lower solidification rate will result in quasi-mushy solidification due to a larger difference in solidification time between surface and center. In the present experiment, however, a clear transition between mushy and quasi mushy solidification was not confirmed.

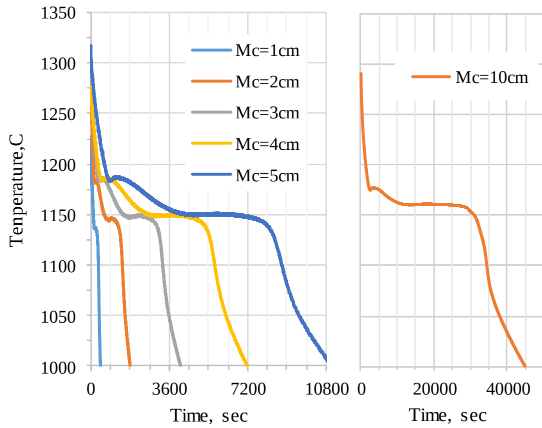


***Fig. 3 Graph shows the solidification curves of cubic test blocks.***

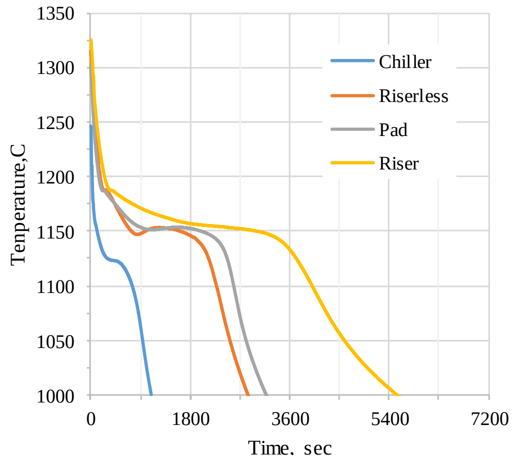


***Fig. 4 Graph shows the solidification curves of plate test blocks.***

## Characterization of the expansion and contraction Behavior

Fig. 6 shows the expansion/contraction behavior. The horizontal axis represents the solidification ratio, and the vertical axis shows the degree of expansion/contraction. Determination of the ratio of each reaction time during the solidification is made possible using the same index by arranging the cooling curves of different solidification times with the solidification ratio as a parameter.

By comparing the expansion/contraction amounts in the reaction of the test samples with various solidification completion times, the contraction of the austenite among the eutectic cells at the end of the solidification tends to decrease against the increase in the solidification completion time.

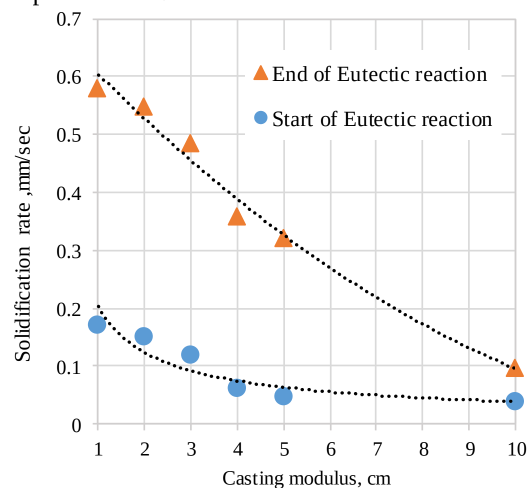


***Fig. 5 Graphical comparison of cooling rate in eutectic reaction each casting modulus.***

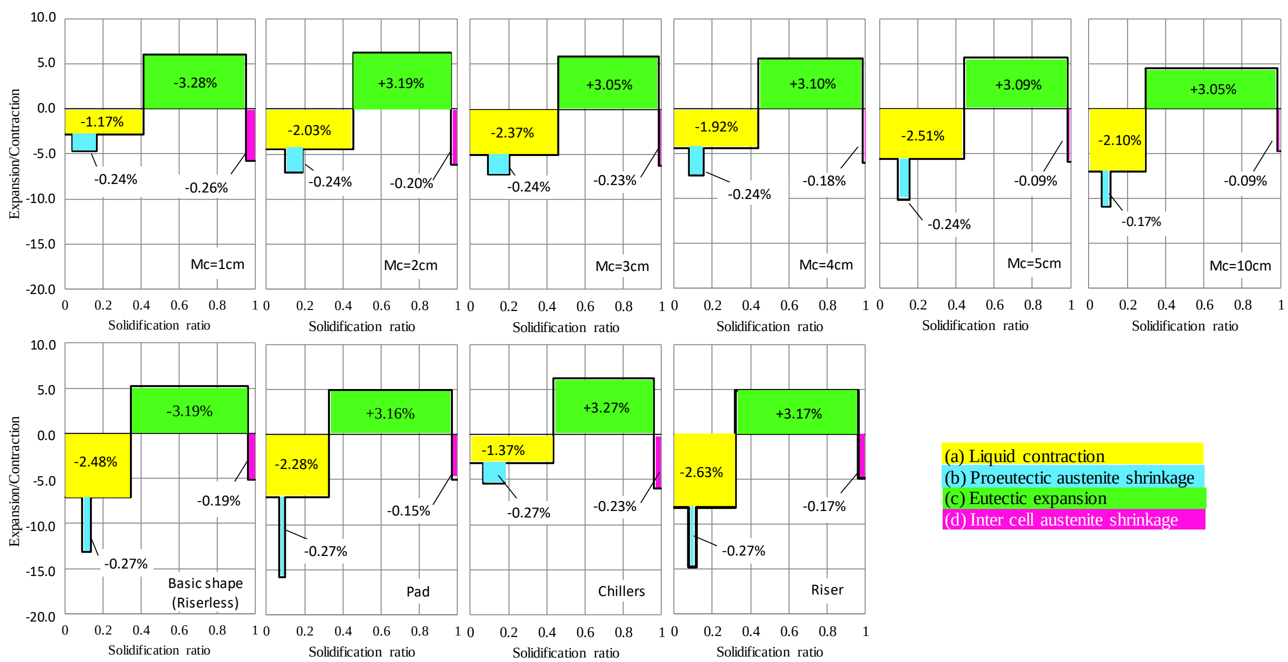


***Fig. 6 Relationship between expansion and contraction at each reaction of cubic and plate test blocks are graphed***

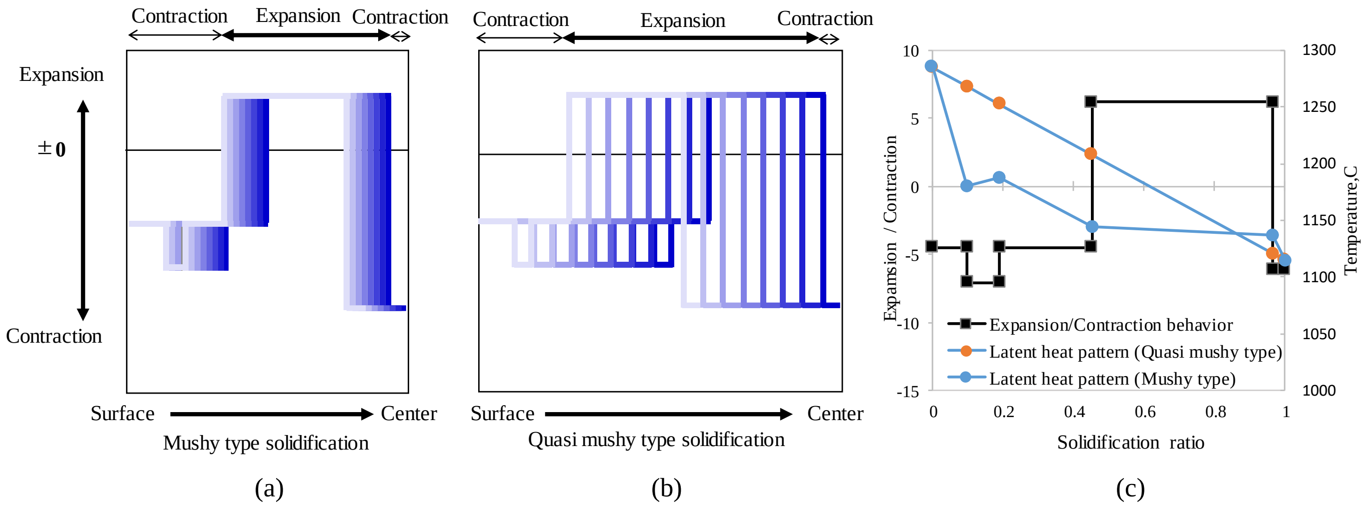


***Fig. 7 These graphs were used in shrinkage cavity analysis; View(a) Conceptual diagram of nominal expansion and contraction behaviour for mushy solidification; (b) Conceptual diagram of nominal expansion and contraction behaviour for quasi mushy solidification; and (c) Latent heat pattern of mushy and quasi mushy type solidification.***

## RESULTS OF THE SHRINKAGE CAVITY ANALYSIS

Based on the results presented in the previous section, the solidification rate is presumed to decrease against the increase of the Mc value, suggesting the shift to the quasi -mushy solidification. By considering the effect of this shift on the expansion/contraction behavior, it can be concluded that the expansion/contraction at the surface and center of the cast simultaneously occurs in the mushy solidification. In the case of the quasi-mushy solidification, there occurs a gap in the expansion / contraction between the surface and center of the cast.

Fig. 7(a) and 7(b) illustrate the conceptual scheme of this model. To apply this concept to the analysis, the change in the latent heat emission is assumed to be constant, is applied to the quasi-mushy solidification, as shown in Fig. 7(c). Consequently, the contraction of the primary crystal and the expansion of the eutectic crystal will speed up, whereas the austenite contraction among the cells was delayed. Therefore, the quasi mushy solidification can be reproduced.

Fig. 8 compares the validation and prediction (I&M's criterion) of the shrinkage cavities for the test blocks. In this study, it was assumed that the shrinkage cavities correspond to 0.0%–99.9% of the predicted values. In the experimental results of the cubic blocks shown in Fig. 8(a), the shrinkage cavities were not formed in any cubic block. This shape of castings is hard normally to see shrinkage in practice. According to B. Chung[2], shrinkage cavity is hardly observed in castings over Mc = 3cm. but is often. Observed in castings less than Mc = 3cm. In this study, castings with Mc=2cm and 3cm had no shrinkage. All cubic casings were poured in one mold therefore sprues were longer than general mold as shown in Fig.1. Higher hydrostatic pressure must be effect for smaller Mc castings. Meanwhile, the prediction results revealed that the shrinkage cavities were forecast to form in the blocks of Mc = 1 cm and 2 cm (0.39 in and 0.79 in). From Fig 5, Mc 1cm and 2cm may take the mushy solidification but not take the quasi-mushy solidification. Therefore, they may not agree with the analysis results. Regarding the results of the plate test blocks presented in Fig. 8(b), the shrinkage cavities were formed in all blocks. Moreover, the prediction of the plate test blocks revealed that the shrinkage cavities were formed in all blocks. The modulus of plate blocks is roughly 2cm.However, it is considered that the temperature gradient of plate block is smaller than that of cube block when the modulus is same. This is because the plate block has a long distance from the surface to the center. That is, it takes semi mushy solidification and the shrinkage tendency agrees to the analysis result.

In the present test condition, our developed prediction method was successfully applied to the cubic blocks larger than Mc = 3 cm (1.18 in.) and all plate test blocks. It is assumed that quasi-mushy solidification applies to heavy castings with long solidification time and with complicated shape. The present method can be applied to actual casting products.

## PREDICTION AND ACTUAL RESULTS OF LARGE HEAVY-SECTION CASTINGS

The expansion/contraction behavior and its prediction method developed in the present study were applied to the actual casting products. Fig. 9 shows the method for determining the expansion/contraction behavior. the difference was calculated between the highest temperature of the non-solidified area and the temperature of the solidus line at the time when all cast surfaces were

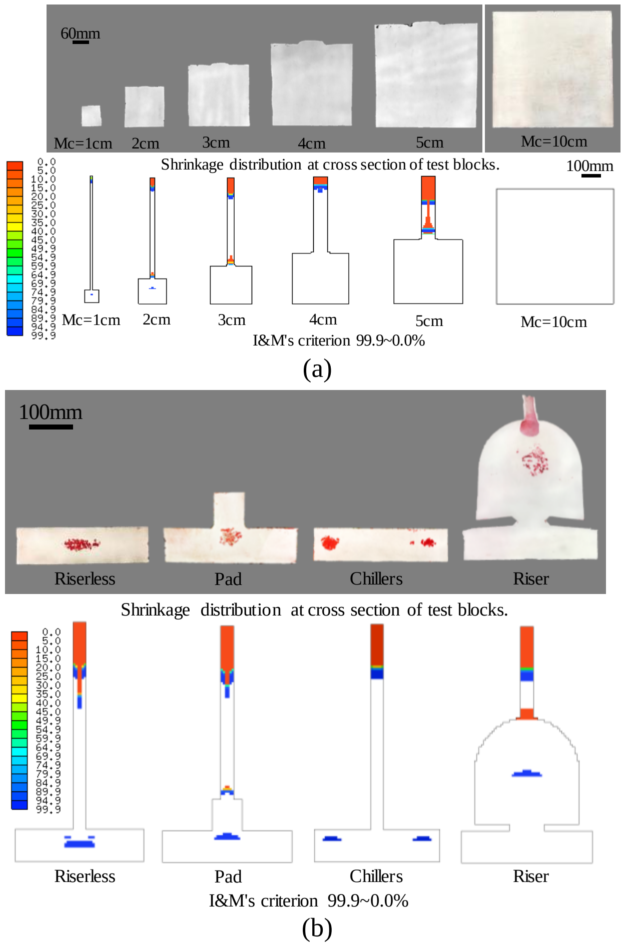


***Fig. 8 The diagram shows the comparison between experimental and simulated result for shrinkage cavity distribution; View (a) cubic blocks; and (b) plate blocks.***

solidified, and the solidified shell was formed. This temperature difference depends on the shape of the cast. In fact, the temperature difference for the plate block was smaller than cubic block in the same modulus value 2cm (0.79in.). The temperature difference was also calculated for the casting products to be analyzed. The expansion / contraction behavior of the test blocks whose temperature difference is closest was applied to the actual casting product. This method is used because of the following reasons. Prior to the formation of the solidified shell, the non-solidified part was in contact with the mold. Therefore, the expansion of the eutectic crystal resulted in the transfer of the mold wall. The shell played the role of a metal mold after its formation. Hence, the eutectic expansion accumulated inside in the non-solidified region. The existence of the shrinkage cavities was determined by the volume balance of the eutectic expansion accumulated inside and the austenite contraction among the eutectic cells at the end of the solidification. Hence, one of the causes of the shrinkage cavity production would be the generation time of the solidified shell. Therefore, if the abovementioned temperature difference is small, the produced amount of eutectic expansion accumulated is small at the end of the solidification process, resulting in the formation of shrinkage cavities. The present study revealed that the temperature difference for the plate blocks was smaller, resulting in the creation of shrinkage cavities.

Fig. 10 presents the external appearance and cross section of the ring-shaped casting product. The filled area is the Ultrasonic testing (UT) area. The hatched part of the riserless design is the region where the flaw echo is observed in the UT area. The flaw detection conditions comprise a probe diameter of 28 mm, frequency of 2.25 MHz, and sensitivity of 6.4 mm (Diameter). In the riser and chiller design, the flaw echo is not observed. Fig. 11 shows the prediction results of the shrinkage cavities. The Niyama criterion is also shown in the Figure for comparison. In both of casting designs, the prediction using our method is closer to the actual prediction results.

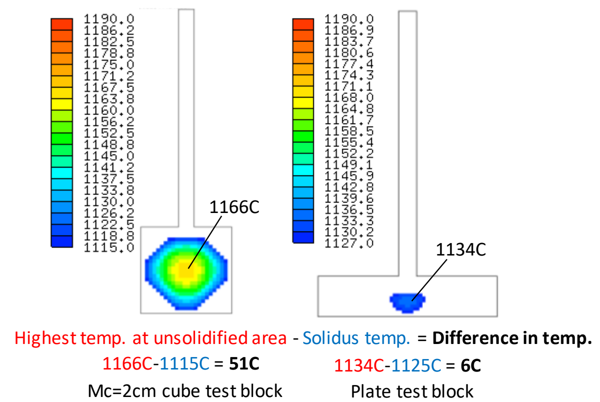


***Fig. 9 Method for determining expansion / contraction behavior by difference between the highest temperature of non-solidified area and solidus temperature when the solidified shell was generated are shown.***

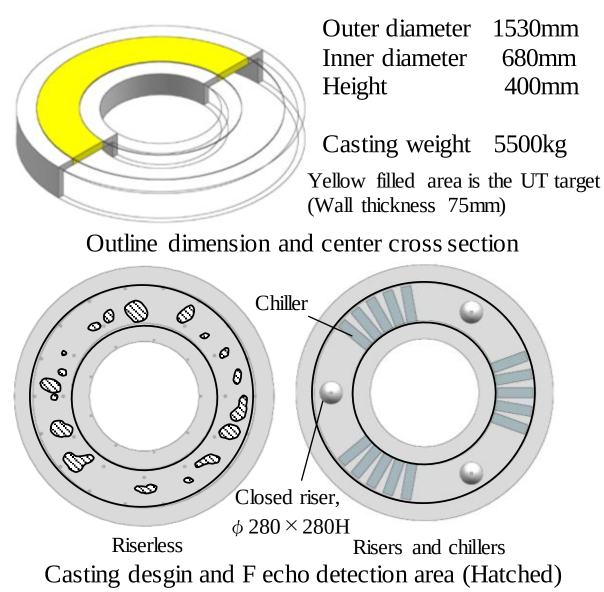


***Fig. 10 Appearance and cross section of the ring-shaped castings and flaw echo detection areas are shown.***

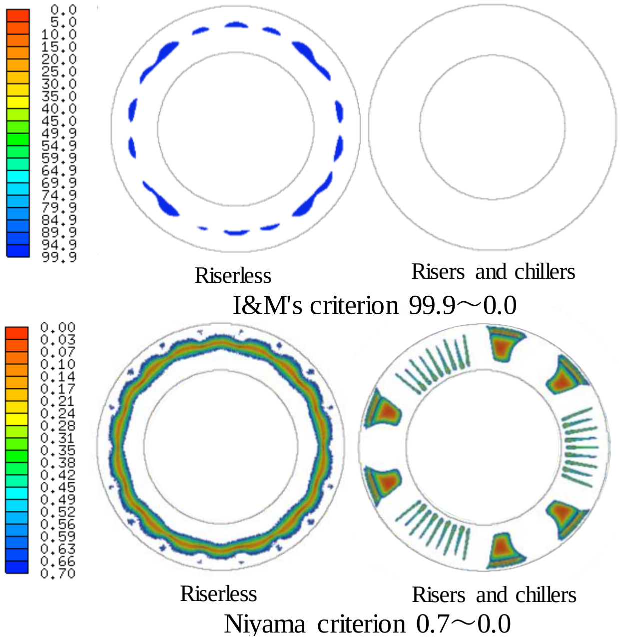


***Fig. 11 Simulation results of the shrinkage cavities are shown.***

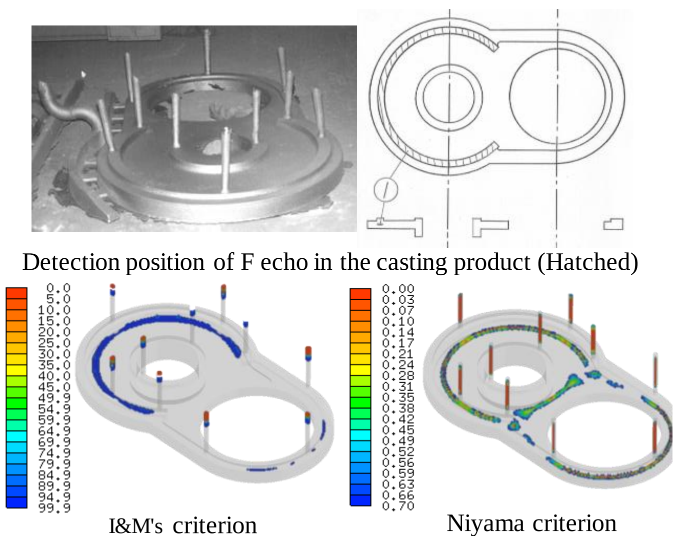


***Fig. 12 Appearance of the plate-shaped casting product and Simulation results of the shrinkage cavities are shown.***

Fig. 12 shows the simulation results of the plate-shaped casting. The size is 1900 mm (74.8 in) × 1200 mm (47.2 in.) × 155 mm (6.1 in.), (Width × Length × Thickness), and the weight is 580 kg (1279 lb.). The hatched part corresponds to the region where the flaw echo was observed in the ultrasonic flaw detection test. The flaw conditions comprise a probe diameter of 28 mm (1.1 in.), frequency of 2.25 MHz, sensitivity of 3.0 mm (0.12 in.), (Diameter), and distance of 250 mm (9.84 in.). Both of casting designs show that the prediction using the present method gives results closer to the reality.

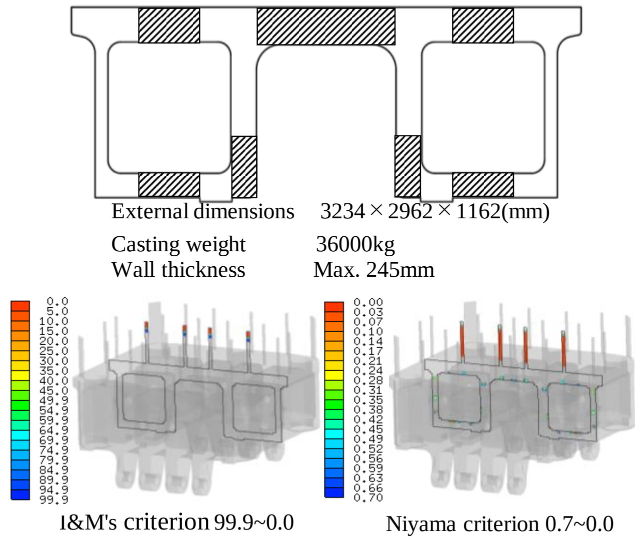


***Fig. 13 Schematic illustration shows the shape and the analysis results of large and heavy section casting product.***

Fig. 13 schematically shows the shape of a large, heavy section casting product and the analysis results. The hatched region represents the important parts in the machine operation. In these regions, neither defects such as shrinkage cavities were observed in the actual evaluation samples and the ultrasonic flaw test. The analysis result was agreement with both the I&M's criterion, wherein the shrinkage cavities are not formed, and the actual experimental results.

## POSSIBILITY OF SHRINKAGE ANALYSIS IN SMALLER CASTINGS

Small castings like wall thickness with less than Mc=3cm may be possible to analyze shrinkage taking similar method if the relationship between the inflection points and the microstructural progress on the solidification curve are understood more. This will be tried in next study.

## CONCLUSION

The volumetric expansion / contraction behavior of solidification was applied to a casting simulation software for heavy section spheroidal graphite iron castings, and the results for the shrinkage cavities were compared with the actual behavior. As the results, the followings were obtained.

(1) The solidification rate of the cubic blocks tended to become smaller against the increase of the Mc value.

(2) The contraction of austenite among the eutectic cells occurring at the end of the solidification tended to become smaller when the solidification time increases.

(3) When the equivalent specific heat method was applied to reproduce the quasi-mushy solidification, the predicted position of the shrinkage cavities for both cubic test blocks having Mc larger than 3 cm (1.18 in) and plate test blocks showed good agreement with the fact.

(4) The precision of shrinkage cavity prediction was improved by the method development in this study. The method can be useful practically to analysis shrinkage when castings have over 3cm of Mc at present.

## REFERENCES


1. Karsay, S.I., "Ductile Iron I-Production," *Quebec Iron and Titanium* (1992).
2. Chang, B., "The Riserless Design of Ductile Cast Iron," *Imono*, vol. 55 pp. 113ff (1983).
3. Taffazzoli, M., Kondic, V., "Making Sound Ductile Iron Castings without Risers," *Foundry Management and Technology* Vol.104 (12), pp. 86ff (1976).
4. Chang, B., Akechi, K., Hnawa, K., *Spheroidal Graphite Cast Iron Basis, Theory, Practice* (1983).
5. Ishikawa, K., Kotani, T., Ogino, T., Itofuji, H., "Effect of Heat Balancer Technique applied for Heavy Section Ductile Iron Castings," 12th Asian Foundry Congress, Taiwan (November 2013).
6. Niyama, K., Uchida, T., Morikawa, M., Saito, S., "A Method of Shrinkage Prediction and Its Application to Steel Casting Practice," *International Cast Metals Journal* Vol.7 (3), pp. 52ff (1982).
7. Yoshida.T., Yano.K., Kawabata,M., "Evaluation of Molten Spheroidal Graphite Cast Iron Shrinkage Tendency by Solidification Time Ratio Between Casting Surface and Inside," *Journal of Japan Foundry Engineering Society* vol.71(2), pp. 104ff (1999).
8. Kim, S., Kwon, E., Roh, D., Yim, Y., "Development of Numerical Model for Improvement of Shrinkage Prediction Accuracy in Ferrous Alloy Castings," 14th Asian Foundry Congress, Korea (November 2017).
9. Sato, A., Iwane, J., Nomoto, S. Ohnaka, I., "Analysis of Residual Deformation of Spheroidal Graphite Cast Iron by Elasto-Plastic VOXEL-FEM," *Journal of Japan Foundry Engineering Society* vol.76 (5), pp.359ff (2004).
10. Hajkowski, J., Roquet, P., Khamashta, M., Codina, E., Ignaszak, Z., "Validation Tests of Prediction Modules of Shrinkage Defects in Cast Iron Sample," *ARCHIVES of FOUNDRY ENGINEERING* vol.17 (Issue1) , pp.57ff (2017).
11. Perzyk, M., Kochański, A., Mazurek,P., Karczewski, K., "Selected Principles of Feeding Systems Design: Simulation vs Industrial Experience," *ARCHIVES of FOUNDRY ENGINEERING* vol.14 (Issue4), pp.77ff (2014).
12. Gwiżdż, A., Pysz,S., Dworak, P., "MAGMAsoft simulation applied in verification of technology to produce new range of alloy steel castings," *ARCHIVES of FOUNDRY ENGINEERING* vol.10 (Issue3), pp.67 (2010)
13. Su, K., Ohnaka, I., Yamauchi, I., Fukusako, T., "Volumetric Change of Columnar Spheroidal Graphite Iron Castings during Solidification," *Journal of Japan Foundry Engineering Society* vol.58 (10), pp.702ff (1986).
14. Yoshida, T., Kawabata, M., "Evaluation of Shrinkage Tendency of Spheroidal Graphite Cast Iron," *Journal of Japan Foundry Engineering Society* vol.70 (5), pp.336ff (1998).
15. Hoched, B., at al., *Diagrammes d'équilibre-Alliages terniaires* (1978).
16. Takahashi, I., Uchida, T., Anzai, K., "Automatic Riser Design by Quantitative Prediction of Shrinkage Cavity," *Journal of Japan Foundry Engineering Society* vol.78 (12), pp.661ff (2006).